ASME Journal of Heat and Mass Transfer
Online journal at:
https://asmedigitalcollection.asme.org/heattransfer

Linyi Xiang
School of Energy and Power Engineering,
Huazhong University of Science and Technology,
Wuhan 430074, China

Bisheng Zhang
School of Energy and Power Engineering,
Huazhong University of Science and Technology,
Wuhan 430074, China

Yuntao Zha
School of Energy and Power Engineering,
Huazhong University of Science and Technology,
Wuhan 430074, China

Guanying Xing
School of Energy and Power Engineering,
Huazhong University of Science and Technology,
Wuhan 430074, China

Xuan Yang
School of Energy and Power Engineering,
Huazhong University of Science and Technology,
Wuhan 430074, China

Zhaochen Wang
School of Energy and Power Engineering,
Huazhong University of Science and Technology,
Wuhan 430074, China

Yanhua Cheng
School of Energy and Power Engineering,
Huazhong University of Science and Technology,
Wuhan 430074, China

Xingjian Yu
School of Energy and Power Engineering,
Huazhong University of Science and Technology,
Wuhan 430074, China

Run Hu
School of Energy and Power Engineering,
Huazhong University of Science and Technology,
Wuhan 430074, China

Xiaobing Luo[1]
School of Energy and Power Engineering,
Huazhong University of Science and Technology,
Wuhan 430074, China
e-mail: Luoxb@hust.edu.cn

Physics-Informed Proper Orthogonal Decomposition for Accurate and Superfast Prediction of Thermal Field

Thermal field prediction has garnered ever-increasing attention as an urgent and vital issue in broad applications ranging from thermal management, performance prognosis, lifetime evaluation, and safety assessment, to energy conversion and carbon neutrality. Suffering from the huge amounts of data and iterative iterations, traditional full-order prediction methods are overstretched for rapid predictions and analysis of complex physical fields. In contrast, reduced-order methods, like proper orthogonal decomposition, can tackle such issues with accelerated computational efficiency but predictions and design may be physically inconsistent or implausible. Here we develop a physics-informed proper orthogonal decomposition for the acceleration of thermal field prediction. By introducing a unified index matrix to reduce the amount of processed data and to uniform the physical equations with the reduced-order equations, we achieve accurate and superfast predictions of thermal fields for unstructured grid, validated by typical complicated spray cooling experiments. The amount of data to be processed achieved a reduction of ten million times, with a maximum computational speedup of 101 times. The physics-informed proper orthogonal decomposition framework is demonstrated to be highly efficient and accurate and can be extended to address a wide range of scientific and technological applications beyond thermal field predictions. [DOI: 10.1115/1.4068266]

Keywords: electronic cooling, heat and mass transfer, jets, wakes, impingement cooling, thermal systems

1 Introduction

Dramatically increased heat flux due to the high-performance demands poses a threat to electronics. Thermal monitoring and prediction of sophisticated electronic devices is often challenging

[1]Corresponding author.

Contributed by the Heat Transfer Division of ASME for publication in the Journal of Heat and Mass Transfer. Manuscript received December 5, 2024; final manuscript received March 15, 2025; published online April 11, 2025. Assoc. Editor: Antonio Jose Silva Neto.

which ensures components protection against high thermal load [1–3]. The most common way of obtaining thermal information is direct measurement by invasive experiments, while significant resources are expended to develop complex test equipment and record excessive data. As a result, there is a growing interest in developing computational algorithm of thermal field [4,5]. Traditional computation tools, such as finite element methods (FEM) and computational fluid dynamics techniques as full-order methods, can certainly be used for thermal field calculation, while the computational costs are vast. The efforts on computational algorithm amelioration have been ongoing and the difficulty of realizing this goal cannot be overstated [6–9].

In order to accelerate calculation, great efforts have been conducted to preserve the character and structure of the original problem while reducing the magnitude of the system [10,11]. As a result, the reduced order models (ROMs) were introduced into the simulation such as Krylov approximation method, balanced truncation method, and orthogonal decomposition reduced order model [12,13], among which the proper orthogonal decomposition (POD) reduced order method has attracted great attention benefiting from the high computational efficiency. In this regard, it must be recognized that low computational cost is only one of the advantages of POD. The self-adaptation of the construction of basis modes makes it easier for POD to deal with nonlinear problems or to be coupled with other disciplinary analyses. POD was first raised in 1901 and shined in the field of fluid flow analysis [14]. However, for quite a while, POD was exclusively used for data handling and feature extraction in statistics and meteorology where physical mechanisms were ignored [15,16]. After deepening the mathematical and physical understanding of the POD methodology, the algorithms for POD have been optimized with enhanced stability and computational efficiency [17–25], which has been revealed to be mostly associated with the selection of snapshots and modes. As such, the POD was used in predicting physical trends in the context of flow mechanics [26,27], thermodynamics [28–30], and structural dynamics [31]. Especially in the field of thermal analysis, POD was employed to analyze the coherent structures of thermal flow field [32], the energetic flow structures, and the boundary conditions through the PIV images and simulation data [33–36]. Afterward, thermal fatigue stresses and enhanced heat transfer modes are elaborated deeply in the field of film cooling [36], jet impingement cooling [37], and turbulent pipe flow [38]. Regrettably, most of them conduct repeated calculations or calculate steady-state results under different operating conditions which do not meet the need for timely transient prediction required by electronics monitoring and prediction. In recent years, Galerkin projection and finite volume method (FVM) [39–46] were utilized to refine and extend the POD method by extrapolation calculations in the research of lithium-ion batteries [39], micro-electronics chips [40], robot [41], and data centers [44,45]. Such methods usually contain four parts, namely, snapshot acquisition, order reducing, extrapolation, and reconstruction which remain separation and limits the computational speedup and the application areas of the methodology. Furthermore, in the thermal analysis region, most of the studies still focus on the effect of flow field on heat flux without thermal field calculation. Purely data-driven models such as image analysis may fit observations very well, but there's no physical basis for that. Therefore, there is a pressing need for integrating fundamental physical laws and domain knowledge to POD extrapolation method. In particular, the treatment of unstructured grids required for three-dimensional complex structures is crucial in POD.

The potential combination of POD, which finding the dominant modes of variation in a given dataset, with FVM for the dynamics of the temporal predictions, is a powerful tool that can be employed to model complex thermal field of electronics with a higher level of accuracy and speed. Given this reason, here, we present physics-informed proper orthogonal decomposition (PIPOD) and introduce unified index matrix (UIM) to quickly and accurately predict the three-dimensional complex thermal field. The PIPOD is a promising tool for learning complex temporal dependencies of thermal field and capture long-term trends in the data. The proposed UIM connects four parts of POD extrapolation method tightly and the ensuing double-order reducing accelerates the model throughout the process. To validate the applicability of PIPOD, we experimentally investigate the thermal field of sophisticated spray cooling system which is one of the most advanced cooling technologies [47,48] and compare the temperature consistency with the prediction by PIPOD. The results confirm the accuracy and great increase in speed of PIPOD. PIPOD has also be proved to contribute to the rapid development of customized thermal management systems. The thermal field reduced-order and prediction framework proposed here can be extended to interdisciplinary challenges.

2 Material and Methods

In the proposed algorithm, we introduce the unified indexing matrix (UIM) and implement the double order reducing for whole-process acceleration based on POD. We integrate (temperature) data and mathematical models and embed physics into POD. The principles of the methods and the way they are coupled to each other will be described in detail in this section and see Supplementary Materials on the ASME Digital Collection for more information about the model setup.

2.1 Proper Orthogonal Decomposition. Proper orthogonal decomposition is a reduced-order method that originated from statistical analysis of vector data. In the POD method, low-dimensional data are used to describe the complex high-dimensional spaces based on the selected orthogonal basis. Assuming that the snapshot of the original physical field is $U(x,t)$, which is a snapshot containing the spatial and temporal characteristics.

$$U(x,t) = \begin{bmatrix} u_{x_1,t_1} & u_{x_2,t_1} & u_{x_3,t_1} & \cdots & u_{x_J,t_1} \\ u_{x_1,t_2} & u_{x_2,t_2} & u_{x_3,t_2} & \cdots & u_{x_J,t_2} \\ u_{x_1,t_3} & u_{x_2,t_3} & u_{x_3,t_3} & \cdots & u_{x_J,t_3} \\ \vdots & \vdots & \vdots & \ddots & \vdots \\ u_{x_1,t_I} & u_{x_2,t_I} & u_{x_3,t_I} & \cdots & u_{x_J,t_I} \end{bmatrix} \tag{1}$$

The J is the total number of measurement points and the I represent the total number of snapshots.

As mentioned before, the original physical field is approximated using the selected orthogonal bases. And an approximate solution $\boldsymbol{U}'$ expressed as

$$\boldsymbol{U}' = \sum_{i=1}^{n} \alpha_i \varphi_i \tag{2}$$

The α_i denotes the coefficients of POD basis, φ_i denotes the POD basis, and n denotes the number of POD basis. The POD bases are mutually orthogonal property:

$$(\varphi_i, \varphi_j) = \delta_{ij} = \begin{cases} 0 & i \neq j \\ 1 & i = j \end{cases} \tag{3}$$

Due to its advantages in identifying nonlinear features, maintaining numerical stability, and ensuring computational efficiency, SVD is employed in this study. The original physical field matrix $\boldsymbol{U}$ can be present as

$$\boldsymbol{U} = \boldsymbol{S}\Sigma\boldsymbol{V}^T \tag{4}$$

where $\boldsymbol{S}$ and $\boldsymbol{V}$ are real orthogonal matrices, Σ is a diagonal matrix with non-negative real elements on the diagonal.

Specifically, when the physical field is the thermal field, Eq. (2) can be expressed as

$$T(x,t) = \sum_{i=1}^{\infty} \alpha_i(t)\varphi_i(x) \tag{5}$$

$$\boldsymbol{T}(x,t) \approx \sum_{i=1}^{n} \alpha_i(t)\varphi_i(x) = \boldsymbol{T}'(x,t) \tag{6}$$

In this work, the x denotes the grid number and t denotes the time.

The $\boldsymbol{T}'(x,t)$ is the approximation of the temperature matrix and the optimal POD bases need to be found. Based on the second-order paradigm, the error E between $\boldsymbol{T}(x,t)$ and $\boldsymbol{T}'(x,t)$ is

$$\begin{aligned} \boldsymbol{E} &= \left[\left(\boldsymbol{T}(x,t) - \boldsymbol{T}'(x,t)\right)^{\mathrm{T}} \cdot \left(\boldsymbol{T}(x,t) - \boldsymbol{T}'(x,t)\right) \right] \\ &= \left[\left(\sum_{i=n+1}^{\infty} \alpha_i(t)\varphi_i(x) \right)^{\mathrm{T}} \cdot \left(\sum_{i=n+1}^{\infty} \alpha_i(t)\varphi_i(x) \right) \right] \\ &= \left[\left(\sum_{i=n+1}^{\infty} \alpha_i(t)^2 \right) \right] \end{aligned} \tag{7}$$

According to Eq. (6)

$$\alpha_i(t) = \varphi_i(x)^{\mathrm{T}} \boldsymbol{T}'(x,t) \tag{8}$$

Therefore, error $\boldsymbol{E}$ can be expressed as

$$\begin{aligned} \boldsymbol{E} &= \left[\left(\sum_{i=n+1}^{\infty} \varphi_i^{\mathrm{T}} \boldsymbol{T}'(x,t) \boldsymbol{T}'(x,t)^{\mathrm{T}} \varphi_i \right) \right] \\ &= \sum_{i=n+1}^{\infty} \varphi_i^{\mathrm{T}} (\boldsymbol{T}'(x,t) \boldsymbol{T}'(x,t)^{\mathrm{T}}) \varphi_i \end{aligned} \tag{9}$$

Then, the covariance matrix $\boldsymbol{R}$ is defined as

$$\boldsymbol{R}(x,t) = \left[\boldsymbol{T}'(x,t) \boldsymbol{T}'(x,t)^{\mathrm{T}} \right] \tag{10}$$

As a result, the error $\boldsymbol{E}$

$$\boldsymbol{E} = \sum_{i=N+1}^{\infty} \varphi_i^{\mathrm{T}} \boldsymbol{R}(x,t) \varphi_i \tag{11}$$

The search of optimal POD basis is transformed into the problem of minimizing error $\boldsymbol{E}$. The Lagrange multiplier λ_i is introduced and construct for the Lagrange function

$$L(\varphi_i) = \sum_{i=n+1}^{\infty} \varphi_i^T \boldsymbol{R}(x,t) \varphi_i - \sum_{i=n+1}^{\infty} \lambda_i (\varphi_i^T \varphi_i - 1) \tag{12}$$

After taking the derivative of Eq. (12)

$$\varphi_i^{\mathrm{T}} \boldsymbol{R}(x,t) \varphi_i = \lambda_i \tag{13}$$

The energy of POD basis can be displayed by λ_i. Up to this point, we have completed the first-order reducing.

2.2 Governing Equations. The PIPOD is a method combined with physical governing equations required for the solution of physical parameters such as the velocity field, pressure field, and thermal field. In this section, the thermal field governing equation and the optimization process are presented.

There are three mechanisms by which heat can transfer through regions, namely, conduction, convection, and radiation heat transfer. The basic principle is shown below:

$$q_{\mathrm{cond},x} = -kA \frac{\partial T}{\partial x} \tag{14}$$

$$q_{\mathrm{conv}} = hA(T_w - T_\infty) \tag{15}$$

$$q_r = \varepsilon\sigma(T_1^4 - T_2^4) \tag{16}$$

Taking the two-dimensional unsteady-state heat conduction transfer as an example, the heat conduction equation is

$$\rho c \frac{\partial T}{\partial t} = \lambda \left(\frac{\partial^2 T}{\partial x^2} + \frac{\partial^2 T}{\partial y^2} \right) + s \tag{17}$$

where the ρ is density, c denotes the specific heat, λ is the thermal conductivity, and s denotes the internal heat source.

Based on POD-Galerkin method, the POD bases are introduced into the heat conduction differential equation

$$\rho c \frac{\partial T}{\partial t} \varphi = \lambda \left(\frac{\partial^2 T}{\partial x^2} \varphi + \frac{\partial^2 T}{\partial y^2} \varphi \right) + s\varphi \tag{18}$$

Discretizing the equation gives

$$\rho c \frac{T^k - T^{k-1}}{\Delta t} \varphi = \lambda \left(\frac{\partial^2 T^{k-1}}{\partial x^2} \varphi + \frac{\partial^2 T^{k-1}}{\partial y^2} \varphi \right) + s\varphi \tag{19}$$

Bringing Eq. (6) into Eq. (19), the system of algebraic equations can be simplified as

$$\boldsymbol{K}' \alpha^k = P' \tag{20}$$

where the α^k is the column vector consisting of n POD basis coefficients at the k time-step, $\boldsymbol{K}'$ is a $n \times n$ matrix, and P' is a column vector with N elements. Then, the thermal field can be predicted by Eq. (8).

The finite volume method and its implicit differential format are applied in this study. Therefore, the stability of the solution is guaranteed.

$$T_P^k = \frac{1}{1 + Fo_\Delta \sum a_{PX}} \left(Fo_\Delta \sum a_{PX} T_X^k + T_P^{k-1} + \frac{s_P \Delta t}{\rho c} \right) \tag{21}$$

where $Fo_\Delta = \lambda \Delta t / \rho c V$ is the grid Fourier number, which can be used to judge the convergence of the display format, and the V denotes the volume of the grid. $a_{PX} = S_{PX}/d_{PX}$ represents the ratio of interface area and distance between node P and adjacent node X. Obviously, a_{PX} is different from the control points of the four adjacent grids in the unstructured tetrahedral grid where the coefficient of Fo_Δ is 4. If the $Fo_\Delta/\Delta t \to \infty$ and the time signature (k) is removed, the interior node equation for the two-dimensional steady-state heat conduction problem can be obtained.

However, the temperature values of all nodes at the current moment must be calculated at the same time, i.e., a system of algebraic equations need to be solved associatively for all control points at moment k. The computational cost increases dramatically compared to the display differential format. We propose a unified matrix to fix this issue, and it will be discussed in Sec. 2.3.

2.3 Establishment of Unified Indexing Matrix and Realization of Double-Order Reducing. As demonstrated before, POD basis φ is in vector form while the governing equations of heat transfer are both in scalar form. The prerequisite for applying POD-Galerkin method is that all the equations should be harmonized into matrix form. On the other hand, solving the implicit differential format equation based on FVM method needs many thermal parameters and specific grid information. Repetitive parameter reading and grid traversal calculations are extremely time-consuming. For the first time, we propose a unified indexing matrix $\boldsymbol{M}$ to solve this problem once and for all.

At first, we take advantage of the sparse matrix to create a matrix $\boldsymbol{M_0}$ with all zeros in all regions except the diagonal. We then go through the process of numbering the different grids and obtaining the positional relationships between the different grids. The positional relationships between the grids are stored by assigning values to $\boldsymbol{M_0}$ and a new matrix is obtained, namely, $\boldsymbol{M_0}'$

$$\boldsymbol{M_0} = \begin{pmatrix} -1 & 0 & 0 & \cdots & 0 \\ 0 & -1 & 0 & \cdots & 0 \\ 0 & 0 & -1 & \cdots & 0 \\ \vdots & \vdots & \vdots & \ddots & \vdots \\ 0 & 0 & 0 & \cdots & -1 \end{pmatrix} \tag{22}$$

where $\boldsymbol{M_0}$ is a $z \times z$ matrix and z denote to the number of grid.

The relative positional relationship between the grids is achieved by assigning a value of 1 to the matrix. Then, the thermal parameters and the specific grid information are waiting to be added.

The unstructured grid is different from the structured grid. The thermal parameters and the specific grid information of unstructured grid may be different for each grid. It cannot be given just one coefficient for all information. We proposed a coefficient μ to describe all needed information for each grid, and the format for μ in different conditions are derived by combining and arranging the coefficients of the governing equations to be solved.

When the grid is on the boundary of the structure

$$\mu = \frac{\kappa S}{V\left(\Delta x + \frac{\lambda}{h}\right)} \tag{23}$$

When the grid is inside the structure

$$\mu = \frac{\kappa S}{V\left(\frac{\lambda_1 \Delta x_2}{\lambda_2} + \Delta x_1\right)} \tag{24}$$

where κ, λ, and h are thermal diffusion coefficient, thermal conductivity, and heat transfer coefficient, respectively. The Δx, S, and V represent the center-of-mass distance of grids, area, and volume. We choose two neighboring grids as examples in Eq. (24) corresponding to the indices "1" and "2," respectively.

As a result

$$\boldsymbol{M} = \mu \boldsymbol{M_0}' \tag{25}$$

The proposed unified indexing matrix $\boldsymbol{M}$ contains the necessary thermal parameters and the grid information in one matrix. Using $\boldsymbol{M}$ to store information not only saves space but also makes it simple and clear to get the relative positions of different grids. Therefore, the problem of solving differential equations of complex structures with a large number of grids and material properties can be fixed. And the governing Eq. (21) can be written as:

$$\boldsymbol{T}^k = \boldsymbol{M}\boldsymbol{T}^{k-1} + F \tag{26}$$

The POD-Galerkin method can be used between matrices

$$\varphi \boldsymbol{T}^k = \varphi \boldsymbol{M} \varphi^{\mathrm{T}} \varphi \boldsymbol{T}^{k-1} + \varphi F \tag{27}$$

The reduced-order extrapolation equation

$$\alpha^k = \boldsymbol{K}\alpha^{k-1} + P \tag{28}$$

In this part, we finish the second-order reducing process which aims to reduce the order of the system of equations. The double-order reducing of PIPOD is achieved through the unified indexing matrix, which greatly reduces the computational cost and unifies the FVM method and POD method. What's more, the utilization of the unified indexing matrix greatly reduces the amount of data that needs to be stored for the computation, further reducing the computational cost.

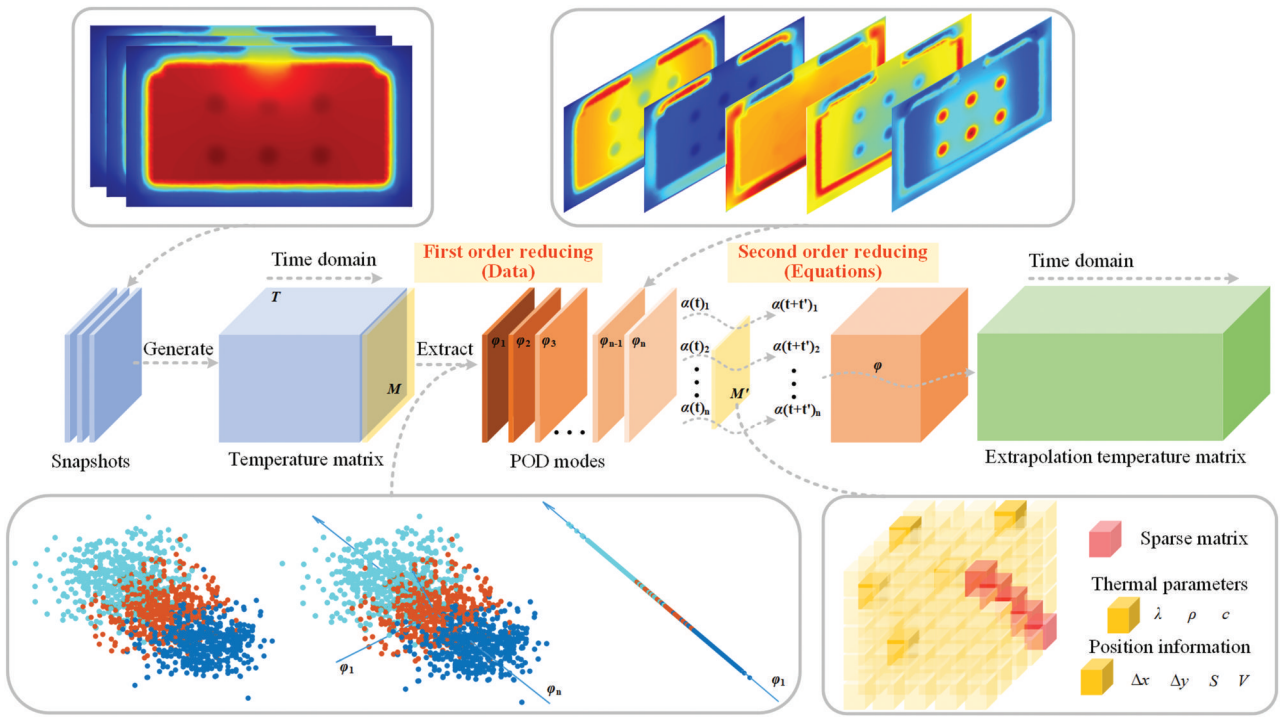

Fig. 1 Overall workflow of the proposed physics-informed POD. *M* refers to the unified indexing matrix, φ refers to the POD basis, and α refers to the coefficient of POD basis. A 2D snapshot of the spray cooling module is shown as an example and the actual snapshot matrix contains temperature field data in 3D. We plot a schematic of the normalized temperature field as an example for the first five POD bases. On the bottom line, the schematic of the extraction stage is given in 3D space and the form and content of the UIM are given.

2.4 Workflow of the Proposed Physics-Informed Proper Orthogonal Decomposition. The workflow of the proposed method for thermal field prediction based on PIPOD is shown in Fig. 1, which concludes collecting snapshots for temperature matrix $\boldsymbol{T}$ in time domain, extracting the POD basis and the coefficients of POD basis, extrapolation of the coefficients of POD basis, and reconstruction of temperature matrix $\boldsymbol{T'}$ in the future time domain. It is worth noting that we take the finite volume method in implicit differential format as solution to get comprehensive temperature field snapshots to create the initial snapshot matrix for order reducing. Especially, we introduce the unified index matrix $\boldsymbol{M}$ containing the thermal parameters and the specific grid information into the temperature matrix. The $\boldsymbol{M}$ can significantly reduce the computational cost by cooperating with sparse matrix and reducing the number of iterations. More importantly, the physical equations are successfully coupled with the POD.

The solution $f(\cdot)$, representing the heat transfer relationship between grids in time domain. The heat conduction is expressed as $f_{\text{cond}}(t^i, \mu^j)$ and the heat convection is expressed as $f_{\text{conv}}(t^i, \mu^j)$, where t^i denotes time of the cycle i, μ^j denotes the coefficient of unified index matrix $\boldsymbol{M}$. A temperature matrix $\boldsymbol{T}$ in time domain can be assembled by the joint solution of $f_{\text{cond}}(t^i, \mu^j)$ and $f_{\text{conv}}(t^i, \mu^j)$. After the temperature matrix has been generated, we use POD to decompose it to obtain the POD basis and the coefficients of POD basis. POD bases are a set of mutually orthogonal vectors, and unlimited basis can be generated theoretically. The greater the number of POD bases, the more information obtained about the original system and the more accurate its reconstructed system will be. Higher-order bases tend to contain higher energy and more information. The accumulated energy $I(N, G)$ is used as a criterion for the selection of bases. The eigenvalues of the real symmetric matrix R are arranged from the largest to the smallest, and select the first N largest eigenvalues in order to minimize the sum of the truncated unreserved eigenvalues G. The process of extraction is shown in Fig. 1, and the numerous separated data are projected onto mutually perpendicular bases. For a given set of POD bases, they will not change over time. We extrapolate the coefficients of POD basis through the UIM. Note that the UIM used here is in the reduced-order extrapolation format after multiplication with the bases. This is a formal unification of physical equations. The newly obtained coefficients of POD basis are multiplied with the original bases to reconstruct the future temperature field.

Obviously, the key to improving computational speed lies in order reducing and UIM. In order to express the principles of acceleration more clearly, the trends in total amount of data with each stage of PIPOD are shown in Fig. 2. We take group no. 2 as example and temperature data for the first 600 s as snapshots. The extrapolated predicted temperature field up to 2000s. The amount of data here is calculated according to the data storage in the form of matrices. If we define a matrix with m rows and n columns, we assume it will contain $m \times n$ data in all. The reduction in data amount is huge as the maximum data amount reaches 7,1780,9400 and the minimum data volume is only 11 throughout the PIPOD calculation. Essentially, we put the most time-consuming part of the computation in the stage with the lowest amount of data, namely, the solving of the $f_{\text{cond}}(t^i, \mu^j)$ and $f_{\text{conv}}(t^i, \mu^j)$. It is also at this stage that we achieve a reduction of the physical equations, eliminating the need to repeatedly solve huge systems of equations. A process that previously required iterative grid-by-grid calculations now requires only the calculation of the coefficients of POD basis for extrapolation. We apply a minimum amount of force to move a heavy weight.

3 Results

3.1 Optimal Estimation of Snapshots, Mode Sets, and Frequencies of Snapshot Sampling. Establishing the above workflow for complex thermal field prediction, we need to further adjust the parameters of the algorithm to make it more stable and efficient. In PIPOD, the snapshots, frequency of snapshot sampling, POD bases, and POD basis coefficient play different roles in the method. As mentioned before, PIPOD contains four parts of snapshot acquisition, order reducing, extrapolation, and reconstruction. The proper combination of above four parameters contributes to the prediction of the thermal field and facilitates coupling to the physical equations. The advantage of POD essentially comes from the omission of secondary information. Thus, there is a coupled competitive relationship. The larger information the samples (snapshots) have, the more comprehensively the changes in the original system are captured, which means more experimental and simulation resources will be consumed. In the present study, it means that the longer temperature needs to be recorded. On the other hand, as mentioned above, the more the POD basis, the more accurate the reconstructed and extrapolated system is, while the more computational cost will be consumed.

Consumption of computational resources will lead to the increase in time. In order to find the optimal modeling framework, we choose three different snapshots to decompose which conclude 200 s, 400 s, and 600 s long temperature data and four frequencies of snapshot sampling including 1, 2.5, 5, and 10. And five POD basis sets are selected according to the accumulated energy $I(N, G)$ of 99%, 99.9%, 99.99%, 99.999%, and 99.9999% (see Supplementary Materials on the ASME Digital Collection for details). Figure 3 illustrates the computational cost of the proposed algorithm based on above three parameters. All the simulations are conducted under standard case (see Supplementary Materials) and extrapolated to 2000s. Order reducing paves the way to make the huge volume of data to a considerable order of magnitude. We try to further accelerate the follow-up process. Overall, the reconstruction is about one hundred times longer than the extrapolation (Figs. 3(*a*)–3(*c*)). The snapshots don't show apparent impact on reconstruction part while tiny reduction of extrapolation time is observed with the increase of snapshots. Similar results are found on the mode sets. The effect extent of the snapshots and mode set in PIPOD is now clear. As front-loading parameters, they will continue to be of little use after the order reducing is complete. This also greatly improves the anticonformity instability of our method.

While time is independent of snapshots and mode sets, we are concerned about the accuracy of the calculations. The f is chosen as 2.5 and temperature of three critical points are compared under experiment, FEM, FVM, and PIPOD with 200 s snapshots,

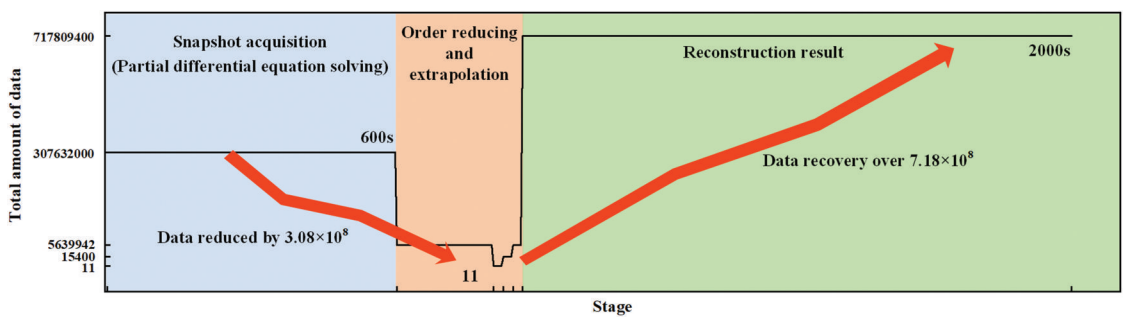

Fig. 2 Trends in total amount of data with each stage

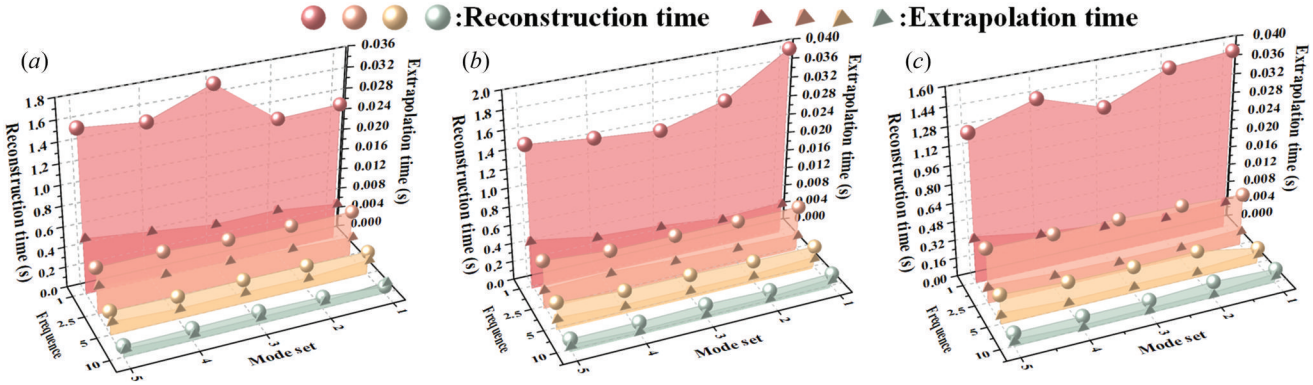

Fig. 3 The reconstruction time and extrapolation time versus frequencies and mode sets: (*a*) 200 s snapshots, (*b*) 400 s snapshots, and (*c*) 600 s snapshots

PIPOD with 400 s snapshots, and PIPOD with 600 s snapshots (Figs. 4(*a*)–4(*e*)).

All five mode sets are tested. When the accumulated energy of the mode set is small, the results obtained from the PIPOD will have a large deviation, especially for short snapshots. Such a problem will be solved as the snapshot increases or the mode set contains more energy. Yet, frequency of snapshot sampling presents an entirely different result. As the f increases, both extrapolation time and reconstruction time decrease substantially (Fig. 3), accompanying maximum reduction are 89.1% and 94.9%, respectively. The reduction of time is not strictly linearly related to the time-step, which we believe is related to matrix multiplication and to the accuracy of the time recording. The error between the standard solution of the FVM and results of the algorithm are used to aid in demonstrating the effect of f (Fig. 4(*f*)). Overall, except for mode set 2 which exhibits an unusually high error, while the absolute values are still within the experimental error. As the mode set increases, the errors show an oscillating downward trend. And we believe that the change of f will not have a huge impact on the accuracy of PIPOD, while it works in time-saving. As postprocessing stages are used for PIPOD, it is surprising that there is such a large effect of extrapolation and reconstruction. Such a coupling description of different parameters is essential for understanding the origins of PIPOD.

3.2 Prediction of the Thermal Characteristics. Spray cooling is a promising thermal management method relying on the high speed, dense droplets hitting the hot surface to dissipate heat. Aerospace, data centers, and many other fields have adopted spray cooling to meet extremely high heat dissipation requirements. However, there are two bottlenecks in the technology iteration process. On the one hand, detecting the temperature field in the future of electronics is indispensable to accurately assess the performance of spray cooling and the status of electronics, while real-time prediction is challenging. On the other hand, the demands of spray cooling system are different for different devices in different circumstances, and it is crucial to quickly match the needs

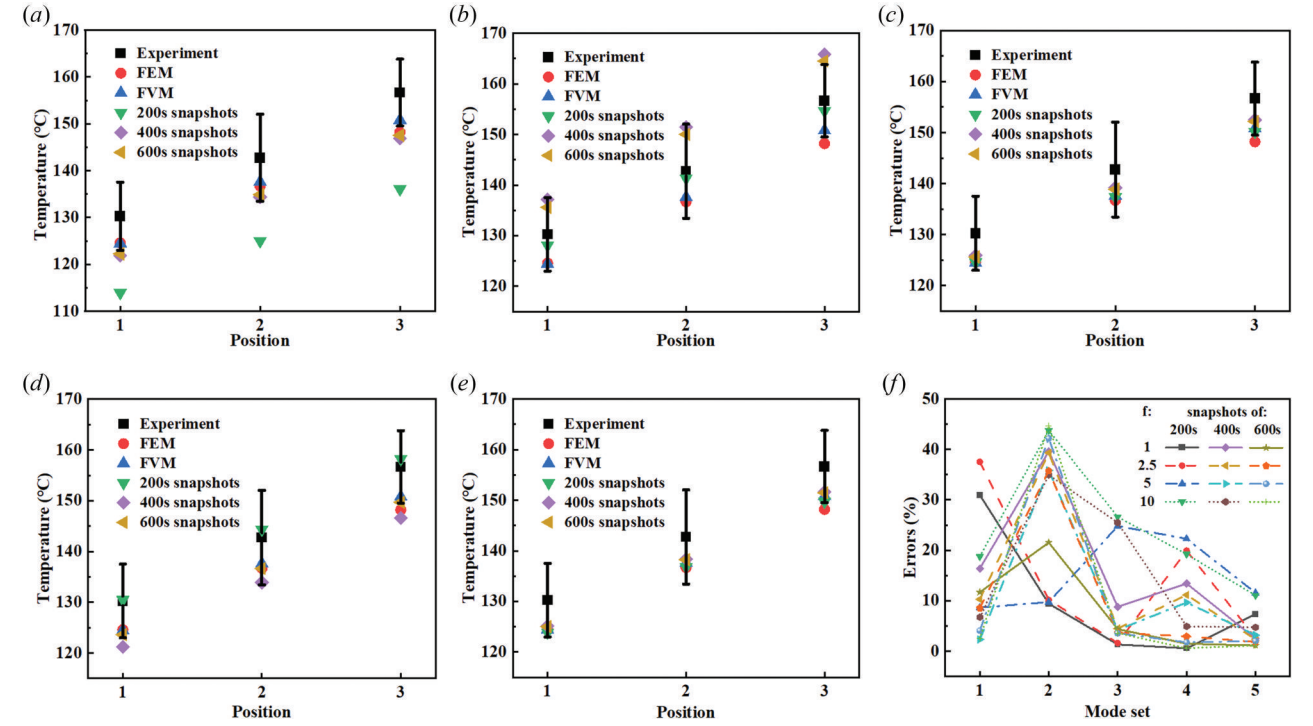

Fig. 4 The temperature and errors of three critical points (see Fig. 6 for the exact location) based on experiment, FEM calculation, FVM calculation, and different snapshots: (*a*) mode set 1, (*b*) mode set 2, (*c*) mode set 3, (*d*) mode set 4, (*e*) mode set 5, (*f*) temperature errors versus mode set which define as the sum of absolute values of relative errors including points 1–3 and maximum temperature

and complete the configuration design in a compact space. Traditional numerical methods can barely solve these bottlenecks considering the cost of time. Thus, the PIPOD method offers a promising alternative to achieve these goals.

In this section, the PIPOD is applied to 21 different cases of spray cooling (see Supplementary Materials on the ASME Digital Collection for details) to validate effectiveness. Different working conditions help to test the stability and applicability of PIPOD. We established a spray cooling system and conducted experimental tests. It is also validated in conjunction with previous experimental results from ourselves and other research teams. Figure 5 gives out the experimental setup and validation of our algorithm. The experimental module with high heat flux is used to create diverse experimental environments and three thermocouples are placed at critical nodes for temperature measurement (Fig. 5(*a*)). The validation of 21 cases for experiment results and calculation results by PIPOD at the three critical nodes are present in two different stages, namely, sample and extrapolation (Fig. 5(*b*)). As we discussed before, the samples (snapshots) are the origin of POD bases and the coefficients of POD basis. Vice versa, the obtained POD bases and the coefficients of POD basis can be used to reconstruct the original temperature field. Therefore, the sample and extrapolation stages are both important in demonstrating the accuracy of PIPOD. In the sample stage, the calculation data are reconstructed by the POD basis and the coefficient of POD basis which can reflect the accuracy of mode extraction. In the extrapolation stage, the data are calculated by PIPOD which can reflect the extrapolating performance of the proposed algorithm. The results show that experiments and PIPOD results have a good agreement with each other in both stages while a maximum relative error of 5.17% appeared in no. 1 and a maximum absolute error of 6.7 °C appeared in no. 8.

The key to spray cooling system design is finding the law of spray cooling enhanced heat transfer. Researchers try to optimize parameters such as volumetric flux, nozzle-to-surface distance, and coolant inlet temperature to maximize the heat transfer coefficient (HTC) or the critical heat flux (CHF). Typically, the two are considered to be in competition with each other and the mission is challenging. In addition to this, the design of the thermal management system, for size, spray orientation, and adaptation to the electronics, is also very important for an effective system. All of these tasks require heat transfer models and correlations which can couple the thermal characteristic parameters with the parameters to be optimized. It has been a long journey from finding the parameters to establishing a single point of connection to forming an associative correlation in two-dimensional [48]. The three most commonly used parameters are Reynolds number (*Re*), Prandtl number (Pr), and Nusselt number (Nu). The reason for the slow progress in this area is that in previous studies, researchers were only able to fit the correlation formula by experimentally measuring data points which is unproductive. The propose of our PIPOD could change that dilemma. We present the distribution of the *Nu* for a certain range of Re and Pr (Fig. 6, color represents the value of *Nu*) in single phase regime. With the advantages of PIPOD, the correlation makes the leap from one unit to whole area. The experimental data are used for validation. The data points behind Fig. 6 are adapted from Rybicki and Mudawar [49] and due to the lack of data in the original literature, we have no way to accurately locate points on the map. But it can be clearly seen that the values of *Nu* in the literature for the same value of Re are in agreement with the values in the map. We can visualize that the effect of *Re* on the heat transfer performance is greater than that of Pr which we needed to count a large number of indices of Re and Pr to reach a conclusion in the past. Further, the flow regime is more important than the velocity and temperature boundary layer thickness. Limited by the dimensions of the plane that can be presented, we have only given rough results, and further research is needed in the future to make finer regional divisions. What's more, this is just one of the applications of PIPOD in thermal

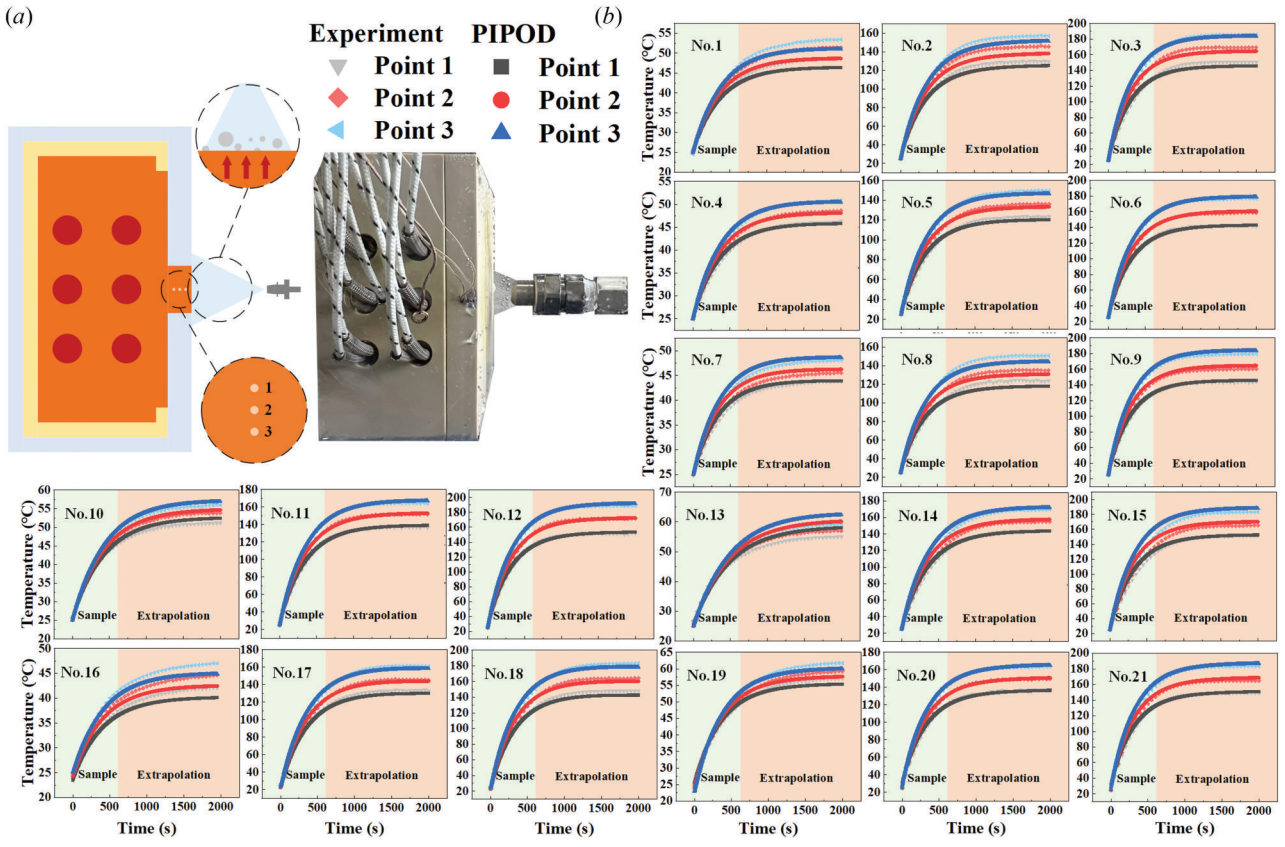

Fig. 5 Experimental setup and validation: (*a*) schematic of the spray cooling module structure, in which high heat flux is generated and (*b*) measured and PIPOD extrapolated temperature of three critical points under 21 cases. The sample is the 600 s snapshots (green region), and all cases are extrapolated to 2000s (orange region).

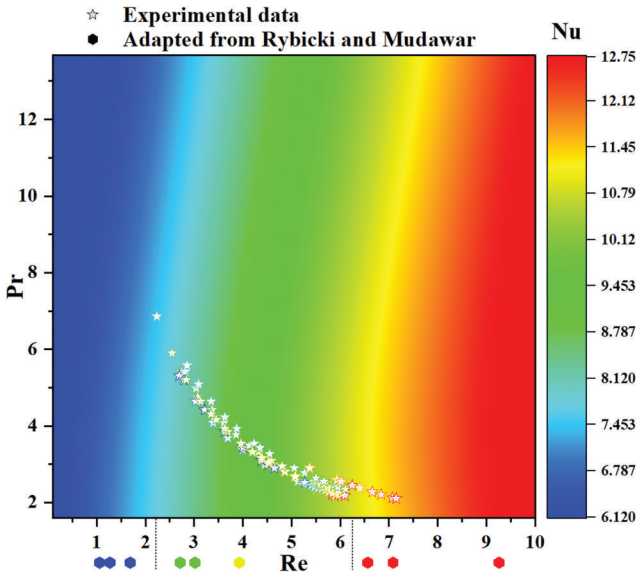

Fig. 6 The range of Nu and distribution of all simulated cases

management system design, and there is still a wide world to be explored.

3.3 Performance of Double Order Reducing of Physics-Informed Proper Orthogonal Decomposition. The traditional POD method accelerates the calculation process by omitting secondary features which is a nonphysical-based calculation. The proposed PIPOD method combines UIM to achieve double order reducing, both for the data and the equations. The UIM is not only for computational speed, it is also a must for combining POD with physical equations solving. As we discussed before, there are four stages in POD extrapolation method. The impact of the PIPOD on each of these four components will be discussed in turn. Although many previous works have employed FVM, FEM, and other numerical methods to obtain snapshots, the amount of data that needs to be processed is completely different from what we are faced with in electronics or thermal management system. Those are 3D models containing hundreds of thousands or even millions of grids. We choose 3 different cases and divide they into nine groups based on the number of grids (see Supplementary Materials on the ASME Digital Collection for details). In fact, we have found out that without UIM, the calculations cannot be executed successfully under exactly the same number of grids and system hardware conditions compared to the standard cases (see Supplementary Materials). Therefore, the calculations are conducted under the condition of reducing the number of grids which means the precision needs to be sacrificed (see Supplementary Materials). Figure 7 shows the comparison of time consumption of PIPOD and the traditional POD in four stages.

As shown in Fig. 7(*a*), the UIM plays a significant role in saving time and the greater the number of grids, the more effective the UIM is in saving time. The UIM improves computation speed up to 299 times. Figure 7(*b*) gives the time consumption of remaining three stages of order reducing, extrapolation, and reconstruction, which are also accelerated vastly. The total time of the calculations are all kept under 10 s in all cases, and PIPOD shows remarkable acceleration. Meanwhile, the time required for full process calculations with FVM is 101 times that of PIPOD based on case 2 (Multiple calculations, under stable computer conditions). Such an increase in speed is exciting and opens the door to a large number of potential applications, in addition to thermal monitoring and thermal design.

4 Discussion

As a reduced-order method, POD has been applied to many areas while the main functions are still image processing and data analysis. In spite of some explorations in the extrapolation algorithm and the combination with Navier–Stokes equations based on POD, it is still very challenging to deal with a complex three-dimensional model that contains heat and mass transfer. The PIPOD creatively introduces the unified index matrix into the POD method, simplifying the numerous physical parameters and complex relative positional relationships. Double order reducing achieving by PIPOD not only reduces the amount of data but also the system of equations to be solved. More importantly, the algorithm described in this work introduced into the physical mechanism and improved the robustness and generality of algorithm. Eventually, we can rapidly predict the three-dimensional complex thermal field and the PIPOD saves thousands of times over traditional methods.

Efficient coupling of mathematical methods and physical equations has far-reaching implications, which can lead to complementary strengths. Physics-informed proper orthogonal decomposition can be leveraged to improve the performance of POD by learning the physical and mathematical understanding of the world. The proposal of UIM provides the idea that matrices can unify not only the complicated parameters but also the form of equations. In this work, we applied the method on POD and FVM based on spray cooling system and offered potential application in thermal monitoring and thermal design. Here, we inherently constrain the thermal design in single-phase regime due to the limited understanding of complex bubble dynamics in the two-phase regime and experimental observational data. It is worthwhile to extend the method to two-phase regime and other advanced thermal

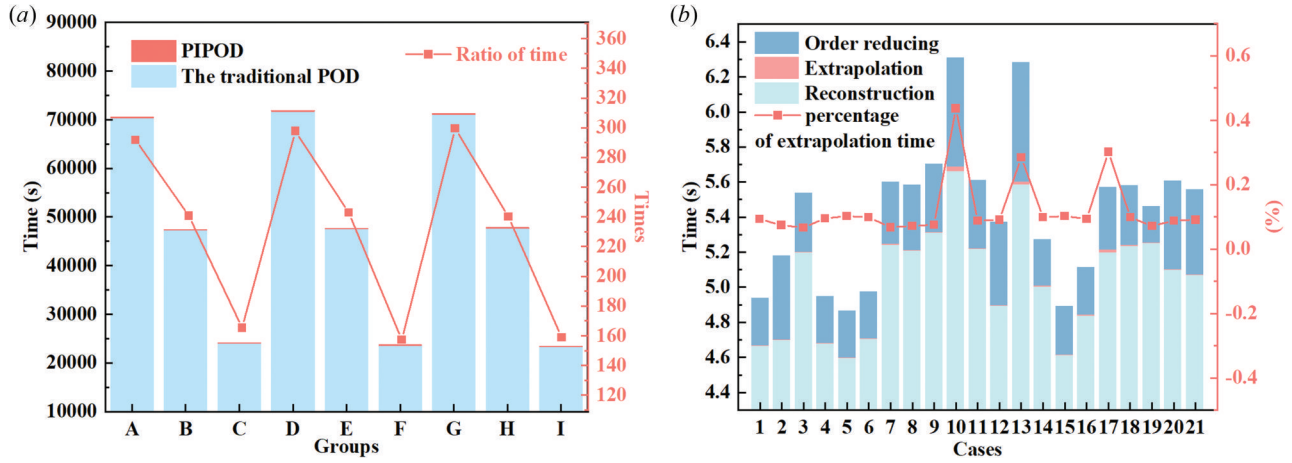

Fig. 7 (*a*) The snapshot acquisition time requirement comparison of PIPOD and the traditional POD method without UIM of different groups and (*b*) the time requirement of order reducing, extrapolation, and reconstruction stage in PIPOD of different cases

management technologies. Thus, with the efficiency bottleneck removed, there are multitude of research directions worth investigating. More broadly, apart from the Navier–Stokes equations, continuity equation, and energy equation, other mathematical, physics, or chemical equations can be introduced such as Maxwell's equations, Gauss's law, and thermodynamic equation. Hopefully, the PIPOD may fuel fundamental theoretical discoveries and applications in more fields such as electromagnetism, optics, and biomedicine.

Funding Data

- National Key R & D Project from Ministry of Science and Technology of China (Grant No. 2022YFA1203100; Funder ID: 10.13039/501100002855).
- National Natural Science Foundation of China (Grant Nos. 52422603, 52076087, and 5221150005; Funder ID: 10.13039/501100001809).
- Natural Science Foundation of Hubei Province (Grant No. 2023AFA072; Funder ID: 10.13039/501100003819).

References

[1] Van Erp, R., Soleimanzadeh, R., Nela, L., Kampitsis, G., and Matioli, E., 2020, "Co-Designing Electronics With Microfluidics for More Sustainable Cooling," Nature, **585**(7824), pp. 211–216.
[2] Luo, X., Hu, R., Liu, S., and Wang, K., 2016, "Heat and Fluid Flow in High-Power LED Packaging and Applications," Prog. Energy Combust. Sci., **56**, pp. 1–32.
[3] Xiang, L., and Hu, R., 2022, "Liquid Directional Steering," Matter, **5**(1), pp. 13–15.
[4] Karim, A., Kim, Y. J., and Kim, J.-H., 2021, "Two-Dimensional Flow Boiling Characteristics With Wettability Surface in Microgap Heat Sink and Heat Transfer Prediction Using Artificial Neural Network," ASME J. Heat Transfer-Trans. ASME, **143**(9), p. 091601.
[5] Du, X., Damewood, J. K., Lunger, J. R., Millan, R., Yildiz, B., Li, L., and Gómez-Bombarelli, R., 2023, "Machine-Learning-Accelerated Simulations to Enable Automatic Surface Reconstruction," Nat. Comput. Sci., **3**(12), pp. 1034–1044.
[6] Fawzi, A., Balog, M., Huang, A., Hubert, T., Romera-Paredes, B., Barekatain, M., Novikov, A., et al., 2022, "Discovering Faster Matrix Multiplication Algorithms With Reinforcement Learning," Nature, **610**(7930), pp. 47–53.
[7] Karniadakis, G. E., Kevrekidis, I. G., Lu, L., Perdikaris, P., Wang, S., and Yang, L., 2021, "Physics-Informed Machine Learning," Nat. Rev. Phys., **3**(6), pp. 422–440.
[8] Wang, F., Zhai, Z., Zhao, Z., Di, Y., and Chen, X., 2024, "Physics-Informed Neural Network for Lithium-Ion Battery Degradation Stable Modeling and Prognosis," Nat. Commun., **15**(1), p. 4332.
[9] Chen, Z., Xiong, R., Lu, J., and Li, X., 2018, "Temperature Rise Prediction of Lithium-Ion Battery Suffering External Short Circuit for All-Climate Electric Vehicles Application," Appl. Energy, **213**, pp. 375–383.
[10] Solera-Rico, A., Vila, C. S., Gómez-López, M., Wang, Y., Almashjary, A., Dawson, S. T. M., and Vinuesa, R., 2024, "β-Variational Autoencoders and Transformers for Reduced-Order Modelling of Fluid Flows," Nat. Commun., **15**(1), p. 1361.
[11] Lu, K., Jin, Y., Chen, Y., Yang, Y., Hou, L., Zhang, Z., Li, Z., and Fu, C., 2019, "Review for Order Reduction Based on Proper Orthogonal Decomposition and Outlooks of Applications in Mechanical Systems," Mech. Syst. Signal. Pr., **123**, pp. 264–297.
[12] Lu, K., Zhang, K., Zhang, H., Gu, X., Jin, Y., Zhao, S., Fu, C., and Yang, Y., 2021, "A Review of Model Order Reduction Methods for Large-Scale Structure Systems," Shock Vib., **2021**, pp. 1–19.
[13] Mignolet, M. P., Przekop, A., Rizzi, S. A., and Spottswood, S. M., 2013, "A Review of Indirect/Non-Intrusive Reduced Order Modeling of Nonlinear Geometric Structures," J. Sound Vib., **332**(10), pp. 2437–2460.
[14] Pearson, K., 1901, "LIII on Lines and Planes of Closest Fit to Systems of Points in Space," London, Edinburgh, Dublin Philos. Mag. J. Sci., **2**(11), pp. 559–572.
[15] Citriniti, J. H., and George, W. K., 2000, "Reconstruction of The Global Velocity Field in The Axisymmetric Mixing Layer Utilizing the Proper Orthogonal Decomposition," J. Fluid Mech., **418**, pp. 137–166.
[16] Sieber, M., Paschereit, C. O., and Oberleithner, K., 2016, "Spectral Proper Orthogonal Decomposition," J. Fluid Mech., **792**, pp. 798–828.
[17] Pawar, S., Ahmed, S. E., San, O., and Rasheed, A., 2020, "Data-Driven Recovery of Hidden Physics in Reduced Order Modeling of Fluid Flows," Phys. Fluids, **32**(3), p. 036602.
[18] Khoo, Z. C., Chan, C. H., and Hwang, Y., 2022, "A Sparse Optimal Closure for A Reduced-Order Model of Wall-Bounded Turbulence," J. Fluid Mech., **939**, p. A11.
[19] Ahmed, S. E., Pawar, S., San, O., Rasheed, A., Iliesuc, T., and Noack, B. R., 2021, "On Closures for Reduced Order Models-A Spectrum of First-Principle to Machine-Learned Avenues," Phys. Fluids, **33**, p. 091301.
[20] Jiang, C., Soh, Y. C., and Li, H., 2017, "Two-Stage Indoor Physical Field Reconstruction From Sparse Sensor Observations," Energy Build, **151**, pp. 548–563.
[21] Bukka, S. R., Gupta, R., Magee, A. R., and Jaiman, R. K., 2021, "Assessment of Unsteady Flow Predictions Using Hybrid Deep Learning Based Reduced-Order Models," Phys. Fluids, **33**(1), p. 013601.
[22] Zhang, J., and Zhao, X., 2020, "A Novel Dynamic Wind Farm Wake Model Based on Deep Learning," Appl. Energy, **277**, p. 115552.
[23] Guastoni, L., Güemes, A., Ianiro, A., Discetti, S., Schlatter, P., Azizpour, H., and Vinuesa, R., 2021, "Convolutional-Network Models to Predict Wall-Bounded Turbulence From Wall Quantities," J. Fluid Mech., **928**, p. A27.
[24] Towne, A., Schmidt, O. T., and Colonius, T., 2018, "Spectral Proper Orthogonal Decomposition and Its Relationship to Dynamic Mode Decomposition and Resolvent Analysis," J. Fluid Mech., **847**, pp. 821–867.
[25] Deng, Z., Chen, Y., Liu, Y., and Kim, K. C., 2019, "Time-Resolved Turbulent Velocity Field Reconstruction Using A Long Short-Term Memory (LSTM)-Based Artificial Intelligence Framework," Phys. Fluids, **31**(7), p. 075108.
[26] Nikolaidis, M.-A., Ioannou, P. J., Farrell, B. F., and Lozano-Durán, A., 2023, "POD-Based Study of Turbulent Plane Poiseuille Flow: Comparing Structure and Dynamics Between Quasi-Linear Simulations and DNS," J. Fluid Mech., **962**, p. A16.
[27] Ding, P., Wu, X.-H., He, Y.-L., and Tao, W.-Q., 2008, "A Fast and Efficient Method for Predicting Fluid Flow and Heat Transfer Problems," ASME J. Heat Transfer-Trans. ASME, **130**(3), p. 032502.
[28] Brunini, V., Parish, E. J., Tencer, J., and Rizzi, F., 2022, "Projection-Based Model Reduction for Coupled Conduction—Enclosure Radiation Systems," ASME J. Heat Transfer-Trans. ASME, **144**(6), p. 062101.
[29] Mahapatra, P. S., Chatterjee, S., Mukhopadhyay, A., Manna, N. K., and Ghosh, K., 2016, "Proper Orthogonal Decomposition of Thermally-Induced Flow Structure in An Enclosure With Alternately Active Localized Heat Sources," Int. J. Heat Mass Transfer, **94**, pp. 373–379.
[30] Bergmann, M., Cordier, L., and Brancher, J.-P., 2005, "Optimal Rotary Control of the Cylinder Wake Using Proper Orthogonal Decomposition Reduced-Order Model," Phys. Fluids, **17**(9), p. 097101.
[31] Rönnberg, K., and Duwig, C., 2021, "Heat Transfer and Associated Coherent Structures of A Single Impinging Jet From A Round Nozzle," Int. J. Heat Mass Transfer, **173**, p. 121197.
[32] Wang, Y., Yu, B., Cao, Z., Zou, W., and Yu, G., 2012, "A Comparative Study of POD Interpolation and POD Projection Methods for Fast and Accurate Prediction of Heat Transfer Problems," Int. J. Heat Mass Transfer, **55**(17–18), pp. 4827–4836.
[33] Shan, F., Fujishiro, A., Tsuneyoshi, T., and Tsuji, Y., 2014, "Effects of Flow Field on the Wall Mass Transfer Rate Behind A Circular Orifice in A Round Pipe," Int. J. Heat Mass Transfer, **73**, pp. 542–550.
[34] Feng, L.-H., Wang, J., and Pan, C., 2011, "Proper Orthogonal Decomposition Analysis of Vortex Dynamics of A Circular Cylinder Under Synthetic Jet Control," Phys. Fluids, **23**(1), p. 014106.
[35] Wang, L., Pan, C., Wang, J., and Gao, Q., 2022, "Statistical Signatures of Component Wall-Attached Eddies in Proper Orthogonal Decomposition Modes of A Turbulent Boundary Layer," J. Fluid Mech., **944**, p. A26.
[36] Cai, T., Peng, D., Yavuzkurt, S., and Liu, Y. Z., 2018, "Unsteady 2-D Film-Cooling Effectiveness Behind A Single Row of Holes at Different Blowing Ratios: Measurements Using Fast-Response Pressure-Sensitive Paint," Int. J. Heat Mass Transfer, **120**, pp. 1325–1340.
[37] Lee, S., and Hassan, Y. A., 2018, "Experimental Study of Flow Structures Near the Merging Point of Two Parallel Plane Jets Using PIV and POD," Int. J. Heat Mass Transfer, **116**, pp. 871–888.
[38] Antoranz, A., Ianiro, A., Flores, O., and García-Villalba, M., 2018, "Extended Proper Orthogonal Decomposition of Non-Homogeneous Thermal Fields in A Turbulent Pipe Flow," Int. J. Heat Mass Transfer, **118**, pp. 1264–1275.
[39] Vuppula, V. K. R., Ramanujam, M., and Runkana, V., 2024, "Reduced-Order Modeling of Conjugate Heat Transfer in Lithium-Ion Batteries," Int. J. Heat Mass Transfer, **227**, p. 125537.
[40] Barabadi, B., Kumar, S., and Joshi, Y. K., 2017, "Transient Heat Conduction in On-Chip Interconnects Using Proper Orthogonal Decomposition Method," ASME J. Heat Transfer-Trans. ASME, **139**(7), p. 072101.
[41] Ying, Z., Zhang, H., Wang, L., and Melnik, R., 2022, "Propulsion Optimization of A Jellyfish-Inspired Robot Based on A Nonintrusive Reduced-Order Model With Proper Orthogonal Decomposition," Bioinspir. Biomim., **17**(4), p. 046005.
[42] Luo, Z., Teng, F., and Chen, J., 2018, "A POD-Based Reduced-Order Crank–Nicolson Finite Volume Element Extrapolating Algorithm for 2D Sobolev Equations," Math. Comput. Simul., **146**, pp. 118–133.
[43] Balajewicz, M. J., Dowell, E. H., and Noack, B. R., 2013, "Low-Dimensional Modelling of High-Reynolds-Number Shear Flows Incorporating Constraints From the Navier–Stokes Equation," J. Fluid Mech., **729**, pp. 285–308.
[44] Athavale, J., Yoda, M., and Joshi, Y., 2019, "Comparison of Data Driven Modeling Approaches for Temperature Prediction in Data Centers," Int. J. Heat Mass Transfer, **135**, pp. 1039–1052.
[45] Ghosh, R., and Joshi, Y., 2013, "Error Estimation in POD-Based Dynamic Reduced-Order Thermal Modeling of Data Centers," Int. J. Heat Mass Transfer, **57**(2), pp. 698–707.
[46] Samadiani, E., and Joshi, Y., 2010, "Multi-Parameter Model Reduction in Multi-Scale Convective Systems," Int. J. Heat Mass Transfer, **53**(9–10), pp. 2193–2205.
[47] Xiang, L., Yu, X., Hong, T., Yang, X., Xie, B., Hu, R., and Luo, X., 2023, "Performance of Spray Cooling With Vertical Surface Orientation: An Experimental Investigation," Appl. Therm. Eng., **219**, p. 119434.
[48] Xiang, L., Cheng, Y., Yu, X., Fan, Y., Yang, X., Zhang, X., Xie, B., and Luo, X., 2023, "High-Performance Thermal Management System for High-Power LEDs Based on Double-Nozzle Spray Cooling," Appl. Therm. Eng., **231**, p. 121005.
[49] Rybicki, J. R., and Mudawar, I., 2006, "Single-Phase And Two-Phase Cooling Characteristics of Upward-Facing and Downward-Facing Sprays," Int. J. Heat Mass Transfer, **49**(1–2), pp. 5–16.